Research in Astronomy and Astrophysics, 25:025014 (8pp), 2025 February

https://doi.org/10.1088/1674-4527/adac92
CSTR: 32081.14.RAA.adac92

Star Formation Efficiency of Blue Compact Galaxies Through (O II), (H_α), (IR), and 1.4 GHz Radio Continuum

Gemechu Muleta Kumssa
Space Science and Geospatial Institute (SSGI), Entoto Observatory and Research Center (EORC), Astronomy and Astrophysics Department, Addis Ababa, Ethiopia; gemechumk@gmail.com
Received 2024 September 19; revised 2025 January 3; accepted 2025 January 19; published 2025 February 10

Abstract

This paper investigates the star formation efficiency (SFE) of blue compact galaxies (BCGs) by analyzing various indicators, including (O II), (H_α), infrared emissions, and the 1.4 GHz radio continuum. The assessment of SFE was conducted using publicly accessible data that concentrated on star formation rates (SFRs) and depletion timescales. By employing the fundamental equation, I determined the SFE in relation to its freefall time, which highlighted variations in efficiencies associated with SFR masses derived from different spectra. The results demonstrated that the highest efficiency value was observed in the analysis of the 1.4 GHz radio continuum, emphasizing the importance of studying star-forming clouds across a range of electromagnetic wavelengths to achieve a comprehensive understanding of star formation mechanisms. The study's findings indicated a peak efficiency of star formation value of approximately 0.9%, while the relative minimum obtained from (O II) was around 0.42%, aligning with the range of SFEs documented in the existing literature. Additionally, investigating the factors that influence the variability in efficiency when examining clouds in BCGs across different wave bands is crucial for deepening our comprehension of the underlying processes of star formation.

Key words: catalogs – methods: analytical – turbulence – shock waves – accretion, accretion disks – stars: dwarf novae

1. Introduction

Blue compact galaxies (BCGs) are situated in the southern constellation of Centaurus, and NGC 5253 stands out as one of the closest blue compact dwarf (BCD) galaxies known to us, positioned approximately 12 million light-years away from Earth (Kunth & Östlin 2000). These galaxies are distinguished by their notable feature of hosting highly active star-forming areas. BCD galaxies are home to molecular clouds (MCs) that bear a striking resemblance to the pure clouds that gave birth to the initial stars in the ancient Universe, lacking any dust or heavier elements. This is why astronomers view these galaxies as a perfect environment for gaining deeper insights into the process of star formation in the early stages of the Universe. BCGs exhibit distinct features such as their blue color, condensed structure, significant gas presence, prominent emission lines from nebulae, and relatively low levels of chemical elements (Kunth & Östlin 2000).

BCD galaxies that are blue in color are known for their active star formation and youthful nature. These galaxies serve as valuable tools for validating theories on galaxy formation, the chemical evolution of matter, and the development of massive stars (Izotov et al. 1990). Izotov et al. (1990) found that observations reveal an exceptionally low abundance of heavy elements in this galaxy, with the oxygen levels being 77 times lower than the solar value and 1.7 times lower than those observed in the previously most deficient galaxy, I Zw 18 (Izotov et al. 1990; Thuan et al. 1996). Additionally, the high electron temperature of 24,800 K suggests the presence of a significant number of stars with masses approximately equal to 100 $M_\odot$ and effective temperatures of ionizing stars reaching up to 8×10^4 K within the galaxy. Based on their observations, SBS0335-052 is in its early stages of development (Izotov et al. 1990; Thuan et al. 1996).

The inquiry into the star formation history of BCGs remains unresolved, as they could be either relatively young galaxies or older galaxies that have experienced a resurgence in star formation activity. In a study detailed in the third paper of a series by Kong (2004), an empirical population synthesis technique was employed, utilizing a library of observed star cluster spectra. The findings indicate that BCGs are typically composed of stellar systems of varying ages, with contributions from young, intermediate-age, and old stellar populations significantly impacting the 5870 Å continuum emission of most galaxies in the sample. Given the presence of old stars in all BCGs examined, the results point toward BCGs primarily being older galaxies with non-continuous star formation histories. The primary objective of numerous ongoing studies in astronomy is to comprehend the history of star formation in the Universe, as highlighted by Madau et al. (1996) and Steidel et al. (1999). Understanding the star formation rate (SFR) is

essential in unraveling the star formation history of galaxies across various redshifts and the overall evolution of the cosmos.

To achieve this comprehension, it is imperative to have a dependable estimation of the SFR in individual galaxies. Several methods for estimating SFR rely on luminosity measurements at different wavelengths, such as radio, infrared (IR), ultraviolet (UV), optical spectral lines (like H_α, [O II] λ 3727), and continuum (Kennicutt 1998). By utilizing these SFR indicators, numerous investigations on the SFR have been conducted at diverse redshift intervals, as demonstrated by studies like Gallego et al. (1995) and Pettini et al. (1998). By employing H_α, [O II]3727, IR, radio (1.4 GHz) luminosities, and neutral hydrogen (H I) gas masses, Kong (2004) conducted calculations to determine SFR and gas depletion times for a sample of 72 star-forming BCGs. However, the authors did not calculate or estimate the star formation efficiency (SFE) or freefall time ($t_{\rm ff}$). Therefore, it is important to investigate the SFE in terms of freefall time ($\epsilon_{\rm ff}$) for these galaxies.

In order to evaluate potential systematic differences among various SFE indicators, I conducted a calculation of the MC mass in the BCG in terms of depletion time and the SFRs obtained from H_α, [O II]3727, IR, and radio luminosities from the catalog of Kong (2004). Additionally, I delved into the calculation of $t_{\rm ff}$ and SFE by considering that the number density of star-forming MC is $n \gtrsim 10^3\,{\rm cm}^{-3}$ as shown by Bertram et al. (2016). This paper examines the SFE of BCGs through the analysis of radio continuum emission, exploring the correlation between SFE and radio continuum. The assessment of the SFR utilizing this approach is also addressed in this work. The purpose of the paper is to study the SFE of BCGs via (O II), H_α, IR emissions, and the 1.4 GHz radio continuum. It is to investigate in which condition we obtain the results of SFE close to the calculated values in the literature.

2. Star Formation

There are many key processes influencing star formation on different scales according to Evans et al. (2009), and the large-scale SFR is determined by physical processes covering a vast range of physical scales. The process of star formation is a fundamental aspect of galaxy formation and evolution, yet it remains inadequately understood within the field of astrophysics (Evans et al. 2009; Kumssa & Tessema 2021). Recent advancements in observational astronomy have yielded a wealth of data regarding the processes of star formation and their subsequent evolution. The intricate dynamics between gravitational forces and opposing pressure forces contribute to the complexity of star formation, making it challenging to achieve a comprehensive understanding of both the mechanisms involved and the SFE (Kumssa & Tessema 2022). Without a robust theoretical framework for star formation, it is difficult to draw conclusions about the origins of life-supporting star systems and their associated planets (Kumssa & Tessema 2022). Various physical processes and pressure forces play a role in star formation across different scales, whether galactic, extragalactic, or at both large and small scales. Notably, the majority of stars are birthed within interstellar clouds, specifically referred to as MCs. There exist numerous approaches to examining the SFE within galaxies. Among these, theoretical and observational methods serve as

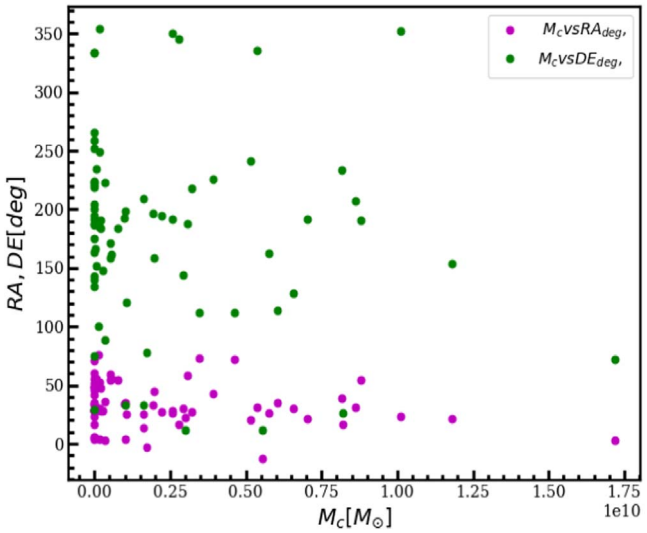

Figure 1. R.A. and decl. vs. MCs in BCGs. This figure indicates the location of the BCGs obtained from the catalog of Kong (2004).

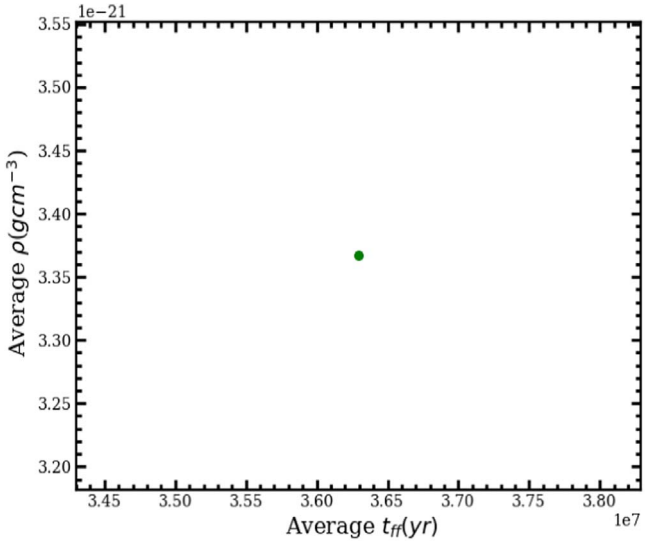

Figure 2. Average $t_{\rm ff}$ time vs. average density of the MC. The average density reached at a specific time is approximately 3.625×10^7 yr, indicating that the density of star-forming galaxies can exhibit significant variation.

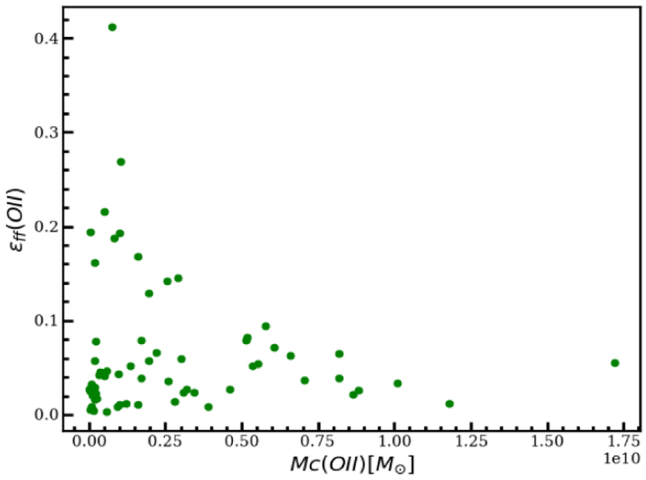

Figure 3. The $\epsilon_{\rm ff}$, as derived from the [O II]3727 emission line, is presented in relation to the cloud mass, denoted as M_c([O II]3727). This figure depicts the $\epsilon_{\rm ff}$ of BCGs, utilizing the cloud mass determined from the observed [O II] values.

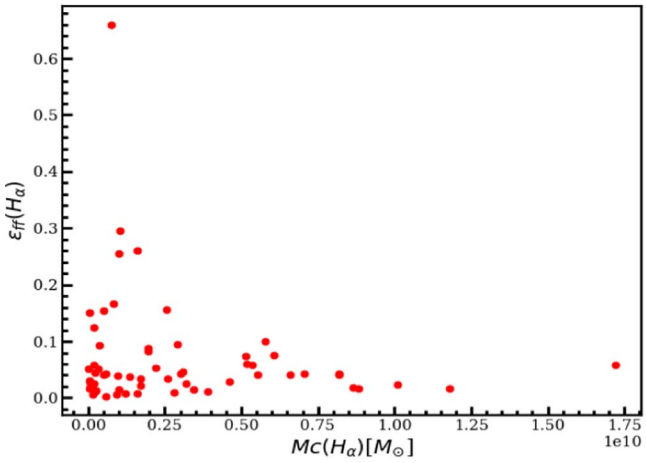

Figure 4. The $\epsilon_{\rm ff}$, as derived from the H_α6563 line, is analyzed in relation to the MC mass, denoted as $M_c(H_\alpha6563)$. This relationship highlights the $\epsilon_{\rm ff}$ determined based on the observed mass values of MCs utilizing the H_α6563 emission line.

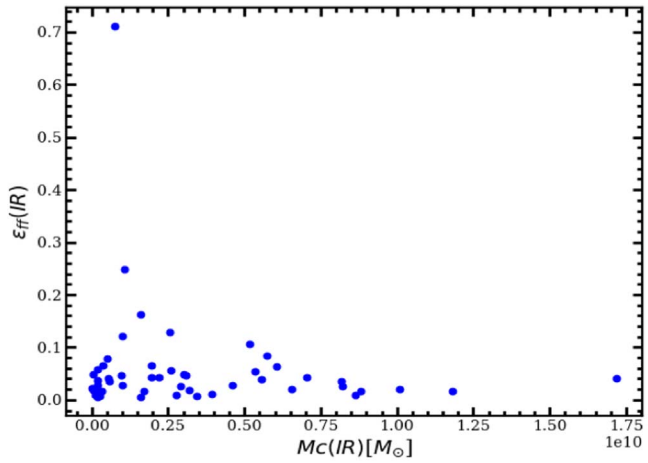

Figure 5. The efficiency of star formation, as derived from IR luminosity in relation to M_c(IR), is illustrated in this figure. It presents the computed $\epsilon_{\rm ff}$ based on the MC mass determined from the observed IR luminosity. Here the $\epsilon_{\rm ff}$ is somewhat in line with the results obtained using (H_α6563).

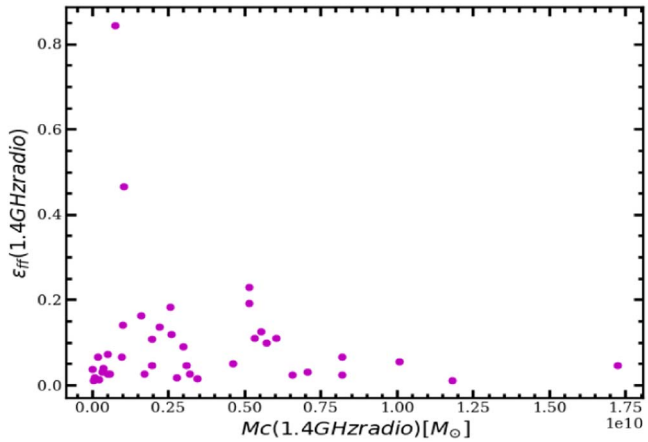

Figure 6. The relationship between the SFR derived from 1.4 GHz radio continuum and the MC mass, denoted as M_c(1.4 GHz radio), is depicted in this figure. It demonstrates the $\epsilon_{\rm ff}$ as a function of the mass of MCs, utilizing data obtained from observations at 1.4 GHz radio frequencies.

foundational elements. In this research, the observed luminosities of H_α, [O II]3727, IR, and radio emissions at 1.4 GHz from BCGs are utilized to analyze and assess the SFE of these galaxies.

These MCs are short lived (10^7-10^8 yr) or long lived (above 10^8 yr) (Fujii & Zwart 2016). Thus all mass in an MC may not be converted to stars efficiently. Studying SFE in MCs will represent an input to developing a consistent star formation theory. Mo et al. (2010) inquired how MCs replace the mass that is converted to stars if the clouds' lifetime is too long and how are they recycled?

3. Star Formation Efficiency

The SFE, both in theoretical models and observational studies, is a topic of great interest and importance in astrophysics. Understanding how stars form and the factors that influence their formation is crucial for unraveling the mysteries of the Universe. By comparing theoretical predictions with observational data, scientists strive to gain insights into the processes that govern star formation and refine our understanding of this fundamental cosmic phenomenon. The BCGs SFR is calculated using depletion timescale and the mass of neutral hydrogen by Kong (2004). However, its SFE has not

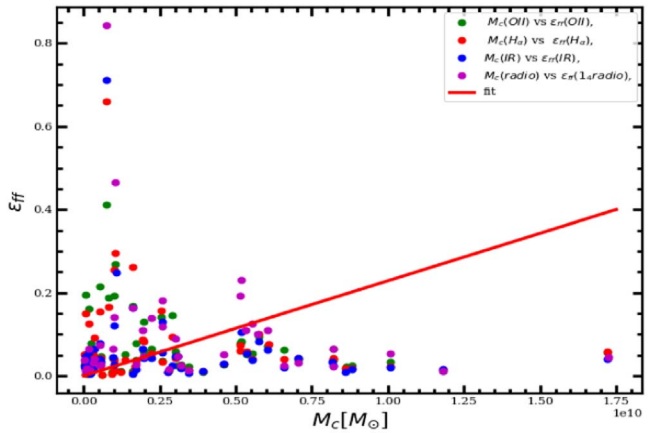

Figure 7. $\epsilon_{\rm ff}$ calculated using M_c from different spectra. The figure illustrates the varying $\epsilon_{\rm ff}$ calculated for each cloud within a BCG. It presents the distribution of observed clouds in relation to their efficiency as measured through H_α, O II, IR, and radio observations. The fitted line indicates the linear relationship or deviations between the mass of the MC and its efficiency.

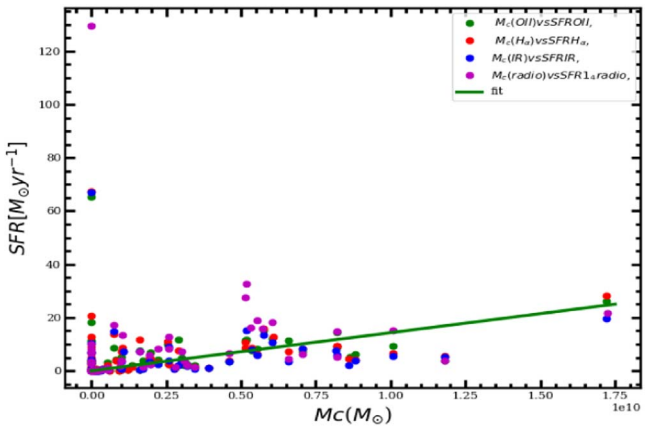

Figure 9. Mass obtained from different spectra vs. the SFR of the respective spectra. The figure illustrates a discrepancy between the SFR and the MC mass, which can be attributed to certain dynamic processes that remain unaccounted for, the surrounding environment of the cloud, and the mechanisms that regulate $\epsilon_{\rm ff}$.

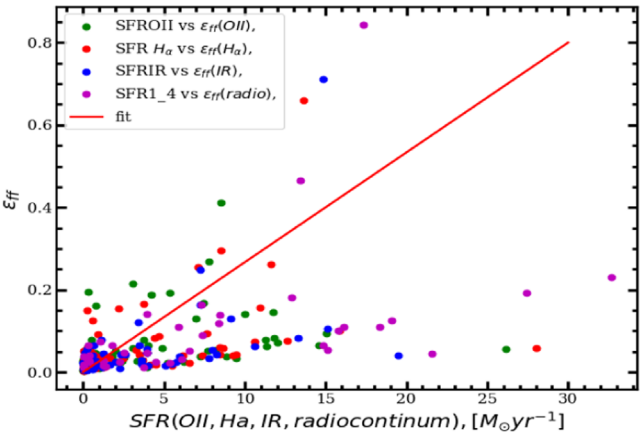

Figure 8. SFR of BCG derived from H_α, [O II]3727, IR, and radio vs. the respective $\epsilon_{\rm ff}$. This illustrates the relationship between $\epsilon_{\rm ff}$ and the SFR of the clouds being examined. As the SFR rises, there is a corresponding increase in $\epsilon_{\rm ff}$.

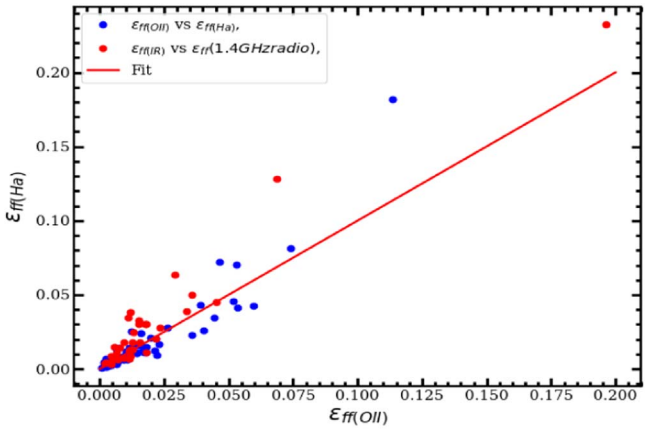

Figure 10. The relation of $\epsilon_{\rm ff}$ calculated using H_α, [O II]3727, IR, and radio (1.4 GHz). The $\epsilon_{\rm ff}$ is rising in both cases but the values are different. The analysis of the fit enables us to understand the relationship between these efficiencies. This understanding is further reinforced when we examine the MCs across various spectra, revealing distinct $\epsilon_{\rm ff}$ associated with those clouds.

been calculated via this method. Therefore, I aimed to calculate the SFE of this cloud in terms of mass of MC by obtaining it assuming SFR and depletion timescale.

Various types of SFE exist, with some based on observational ease and others on theoretical foundations. The definitions of SFE and the parameters used to calculate them are summarized, with a focus on individual gas clouds rather than larger regions or entire galaxies. It is noted that the SFE at the scale of gas clouds can be independent of the SFE integrated over a broader area, as seen in feedback-regulated models related to the Kennicutt (1998) relation by various authors. One of the cloud-scale SFEs is the "integrated" SFE, representing the proportion of gas mass transformed into stars throughout a cloud's lifespan (Murray 2011)

$$\epsilon_{\rm int} = \frac{M_\star(t=\infty)}{M_{\rm gas}(t=0)}, \quad (1)$$

where $M_\star$ is the total mass in stars formed and $M_{\rm gas}$ is the total gas mass, $\epsilon_{\rm int}$ is the integrated SFE which is of particular interest because it is sensitive to the details of stellar feedback physics, as eventually a sufficient number of massive stars will form to expel the gas. $\epsilon_{\rm int}$ ultimately determines the mapping between the MC and star cluster mass functions in a galaxy,

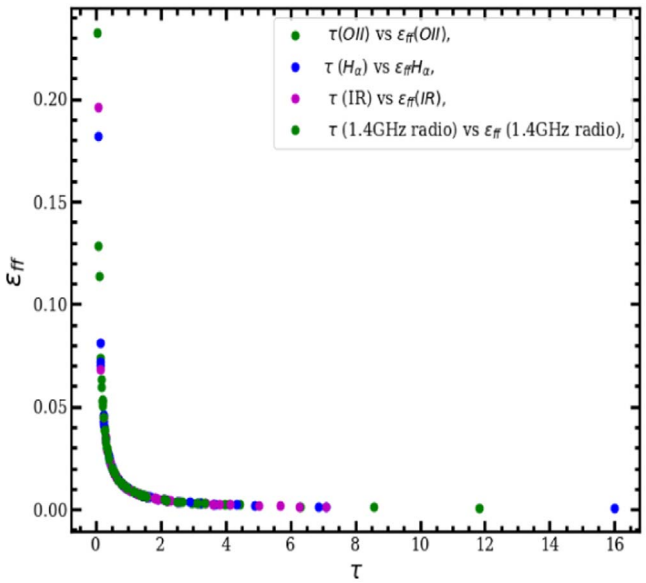

Figure 11. The relationship between τ and $\epsilon_{\rm ff}$ within the context of BCGs indicates that as the duration of depletion extends, the $\epsilon_{\rm ff}$ diminishes in both scenarios. This decline can be attributed to the potential dispersal of the cloud over an extended timeframe.

and dictates the fraction of stars remaining in a gravitationally bound cluster after gas expulsion.

The determination of the instantaneous SFE (ϵ) can be achieved by quantifying the proportion of stars linked to the star-forming cloud at a specific moment in time, as stated by Myers et al. (1986)

$$\epsilon = \frac{M_\star(t)}{M_\star(t) + M_{\rm gas}(t)}. \tag{2}$$

ϵ will evolve from 0 to some finite value during the star-forming lifetime of a cloud, so a certain amount of scatter in this quantity is expected even for a population of clouds with identical properties. As $t \rightarrow \infty$, $\epsilon \rightarrow \epsilon_{\rm int}$. The natural timescale for the evolution of self-gravitating objects is the gravitational $t_{\rm ff}$, and given by

$$t_{\rm ff} = \sqrt{\frac{3\pi}{32G\rho}}, \tag{3}$$

where ρ is the volume-averaged density of the cloud, and G is the gravitational constant. Thus, the $\epsilon_{\rm ff}$ in $t_{\rm ff}$ as described by Krumholz & Tan (2007) is

$$\epsilon_{\rm ff} = \frac{\dot{M}_\star(t) t_{\rm ff}(t)}{M_{\rm gas}(t)}, \tag{4}$$

where $\dot{M}_\star$ represents the rate at which mass from the envelope is falling onto the core that is undergoing star formation. These theories typically predict $\epsilon_{\rm ff} \sim$ 1% for MCs with properties similar to those observed in local spiral galaxies (Bolatto et al. 2008), solely from the properties of isothermal supersonic turbulence plus a gravitational collapse criterion. Because these physics are scale-free, this could potentially explain the observation that $\epsilon_{\rm ff} \sim 1\%$ on a wide range of scales from galaxies to dense star-forming clumps (Krumholz et al. 2011).

The study by Mac Low (2016) stated that gravitational collapse seems more dominant, but the question is how efficient it is, what parameters made the fluctuation of SFE, and to what extent temperature and radius raise and reduce, respectively, to obtain a more efficient MC under its own gravity. Results from various studies show that efficiency ranges from ϵ = 0.030–0.6 over giant molecular clouds (GMCs) regardless of the consideration of dense gas and diffuse gas in MC and $\epsilon \sim 0.5$ for dense gas $n \sim 10^5$ cm^{-3} as Evans et al. (2009) conducted the investigation of the Spitzer Legacy program for a set of five star-forming regions in cores to disks. Similar values were obtained by Heiderman et al. (2010) in 15 additional clouds from the Gould's Belt Survey, but some higher values of $\epsilon_{\rm ff} \approx$ 0.14–0.24 were obtained by Murray (2011). Most of the mass is in large MCs as mass spectra of GMCs show, which leads to lower densities of $\epsilon_{\rm ff} \sim 0.001$–$0.003$ (Krumholz & Thompson 2013). Efficiencies obtained by different scholars vary. In this paper, we study what causes the difference in efficiencies mentioned in Section 1.

In this paper I intend to apply H_α, [O II]3727, IR, and radio (1.4 GHz) luminosities of the star-forming BCGs estimated by Kong (2004). The studies by Murray (2011) and Robitaille & Whitney (2010) estimate SFR in the Milky Way scale and indicate the galactic SFR is $\approx 2 M_\odot\,{\rm yr}^{-1}$; as of the study by Solomon et al. (1987) the total molecular mass of the Milky Way is roughly $10^9 M_\odot$ and efficiency is estimated to be $\epsilon_{\rm ff} \sim 0.01$ (Krumholz & McKee 2005; Krumholz & Tan 2007). Furthermore, García-Burillo et al. (2012) analyzed observations and reported $\epsilon_{\rm ff} \sim 0.01$ using tracers of dense gas with $n \sim 10^5$ cm^{-3} like HCN. Additionally, Murray (2011) obtained Galaxy wide average SFE per $t_{\rm ff}$ and found 0.0057 using the $t_{\rm ff}$ assumed by Krumholz & Tan (2007) which is $t_{\rm ff} = 4.4$ Myr. As Evans et al. (2009) stated, clouds in higher-density regions subtend smaller volumes and include smaller masses. $\epsilon_{\rm ff}$ is nearly constant because $M_{\rm gas}$ and $1/t_{\rm ff}$ both fall with density at about the same rate.

4. Results and Analysis

Starting from the fundamental definition of SFE I aim to calculate SFE of BCG based on the data of Kong (2004). Here I consider the following formulations of SFE

$$\tau = \frac{M_c}{\dot{M}}. \tag{5}$$

In this context, τ represents the depletion timescale, while M_c denotes the mass of the cloud being considered. Additionally, $\dot{M}$ signifies the SFR. From this information, I derive the

Table 1
Calculated Masses of the MC in BCG in Different Spectra and the Corresponding $\epsilon_{\rm ff}$ Using Catalog of Kong (2004) as a Reference

M_c(O II) ($M_\odot$)	M_c(H_α) ($M_\odot$)	M_c(IR) ($M_\odot$)	M_c(radio) ($M_\odot$)	$\epsilon_{\rm ff}$(O II) (%)	$\epsilon_{\rm ff}$(H_α) (%)	$\epsilon_{\rm ff}$(IR) (%)	$\epsilon_{\rm ff}$(radio) (%)
3.00184294E+09	3.00669210E+09	3.00428006E+09	3.00226509E+09	5.940E-02	4.205E-02	4.775E-02	8.961-02
5.53508813E+09	5.53334477E+09	5.54167501E+09	5.52769024E+09	5.369E-02	4.037E-02	3.923E-02	0.125
8.19284378E+09	8.20386304E+09	8.19722394E+09	8.20215398E+09	6.469E-02	4.091E-02	2.563E-02	2.35E-02
1.61395200E+09	1.61545805E+09	1.61016602E+09	1.61197402E+09	0.1680	0.2611	0.1634	0.164
1.00937203E+09	1.01203398E+09	1.00932602E+09	1.01103802E+09	0.1930	0.2556	0.1217	0.141
1.72117627E+10	1.72208579E+10	1.71900723E+10	1.72384010E+10	5.507E-02	5.911E-02	4.119E-02	4.53E-02
1.70817600E+09	1.71674995E+09	1.71093299E+09	1.70700595E+09	7.959E-02	3.456E-02	1.678E-02	2.67E-02
348624000.	349272000.	349440000.	348996000.	4.497E-02	9.259E-02	6.481E-02	3.96E-02
3.45221478E+09	3.43749990E+09	3.45322291E+09	3.45633613E+09	2.364E-02	1.451E-02	6.380E-03	1.46E-02
4.60058419E+09	4.60624998E+09	4.61092454E+09	4.60605594E+09	2.653E-02	2.903E-02	2.869E-02	5.16E-02
6.04648806E+09	6.06576026E+09	6.04598989E+09	6.02535987E+09	7.201E-02	7.561E-02	6.367E-02	0.110
1.04868000E+09	1.05152698E+09	1.05397402E+09	1.04808602E+09	0.2688	0.2950	0.2486	0.465
6.58447309E+09	6.57337293E+09	6.56472269E+09	6.57377485E+09	6.247E-02	4.064E-02	2.013E-02	2.47E-02
1.17988403E+10	1.18005944E+10	1.18210673E+10	1.18145423E+10	1.221E-02	1.685E-02	1.573E-02	1.15E-02
520296000.	520852000.	518420000.	520460000.	0.2160	0.1537	7.890E-02	7.39E-02
1.96531405E+09	1.96159603E+09	1.95868902E+09	1.96211597E+09	0.1291	8.211E-02	4.315E-02	4.66E-02
563601024.	562644992.	563286016.	562325056.	4.707E-02	4.225E-02	3.466E-02	2.67E-02
5.76338381E+09	5.74592717E+09	5.75207987E+09	5.72051712E+09	9.476E-02	9.998E-02	8.401E-02	9.99E-02
19012000.0	18981000.0	19020000.0	19020000.0	2.672E-02	5.162E-02	2.289E-02	3.81E-02
521556000.	522100000.	522375008.	522192032.	4.091E-02	3.997E-02	4.148E-02	2.55E-02
750640000.	749374976.	755718016.	744588032.	0.4124	0.6599	0.7116	0.844
215090000.	214802016.	214964992.	215055008.	2.311E-02	1.132E-02	1.435E-02	1.36E-02
3.07664102E+09	3.07788006E+09	3.08412006E+09	3.08051994E+09	2.414E-02	4.653E-02	4.653E-02	4.68E-02
7.03852493E+09	7.04413594E+09	7.03777024E+09	7.04872448E+09	3.722E-02	4.341E-02	4.265E-02	3.15E-02
2.57759206E+09	2.57879987E+09	2.58130893E+09	2.58340506E+09	3.572E-02	3.456E-02	5.558E-02	0.118
977665024.	984200000.	978467008.	979824000.	4.295E-02	3.923E-02	4.588E-02	6.62E-02
2.22052992E+09	2.21872512E+09	2.21694694E+09	2.21866803E+09	6.587E-02	5.377E-02	4.255E-02	0.138
1.95425997E+09	1.94937600E+09	1.94901606E+09	1.95016806E+09	5.761E-02	8.724E-02	6.458E-02	0.109
3.20160000E+09	3.20100019E+09	3.19829402E+09	3.20234394E+09	2.720E-02	2.494E-02	1.896E-02	2.55E-02
327835008.	328300000.	328263968.	327690976.	4.196E-02	5.185E-02	1.636E-02	3.06E-02
8.19070208E+09	8.18895514E+09	8.17587814E+09	8.19380122E+09	3.932E-02	4.196E-02	3.443E-02	6.56E-02
5.17365606E+09	5.15766374E+09	5.15872819E+09	5.16312422E+09	8.286E-02	5.969E-02	0.1061	0.229
173924992.	174290000.	173900992.	174116000.	0.1613	0.1251	5.697E-02	6.58E-02
5.34510899E+09	5.35550413E+09	5.35463987E+09	5.33082010E+09	5.237E-02	5.848E-02	5.417E-02	0.109
2.78720000E+09	2.78097613E+09	2.78049997E+09	2.78144026E+09	1.395E-02	9.906E-03	8.745E-03	1.670E-02
2.55488026E+09	2.55437901E+09	2.56553011E+09	2.56729907E+09	0.1414	0.1577	0.1297	0.182
1.00895519E+10	1.00908216E+10	1.00924877E+10	1.00781158E+10	3.401E-02	2.378E-02	1.981E-02	5.433E-02

following

$$M_c = \dot{M}\tau. \tag{6}$$

Equation (6) indicates that the gas depletion time influences the SFR. This suggests that as the depletion time increases, the rate of mass infall onto the star-forming core diminishes, resulting from a gradual reduction in the supply of materials from the surrounding disk over time.

4.1. Mass of the MCs of BCGs from Depletion Timescale and SFR

The masses of the MCs can be obtained from depletion timescales and SFRs described in Kong (2004) (Table 1). Those are Gas depletion timescale from [O II]3727, Gas depletion timescale from H_α6563, Gas depletion timescale from IR and Gas depletion timescale from 1.4 GHz continuum, using SFR from [O II]3727, SFR from H_α6563, SFR from IR luminosity and SFR from 1.4 GHz radio 1.4 GHz continuum respectively.

Following this I calculated the MC mass from the depletion timescale and the SFR from the data as:

$$M_c(\text{O II}) = \dot{M}\,[\text{O II}]\,\tau\,[\text{O II}], \tag{7}$$

$$M_{\rm H_\alpha} = \dot{M}\,(\rm H_\alpha)\,\tau\,(\rm H_\alpha), \tag{8}$$

$$M_{\rm IR} = \dot{M}\,(\rm IR)\,\tau\,(\rm IR), \tag{9}$$

$$M_{\rm 1.4\ GHz} = \dot{M}\,(\text{1.4 GHz radio})\,\tau\,(\text{1.4 GHz radio}), \tag{10}$$

where M_c(O II), M_{c2}, M_{c3} and M_{c4} are MC masses in the BCG calculated from the respective SFRs $\dot{M}$ [O II], $\dot{M}$ (H_α), $\dot{M}$ (IR), $\dot{M}$ (1.4 GHz radio) and depletion times τ[O II], τ(H_α), τ(IR), τ(1.4 GHz radio). Now considering the particle number

density of the cloud is $n = 10^3\,\mathrm{cm}^{-3}$, we can obtain the initial density of the cloud by applying the density given as

$$\rho = n\mu m_{\mathrm{H}}, \tag{11}$$

where $\mu = 2.016$ is the mean molecular weight and m_{H} mass of hydrogen.

Figure 1 shows the location of the star-forming clouds in BCGs in terms of decl. (J2000) and R.A. (J2000) from the data of Kong (2004). Figure 2 implies the average t_{ff} time calculated from the assumed average density.

4.2. Star Formation Efficiency of Blue Compact Galaxy in Freefall Time

In this section, I intend to calculate the SFE of a BCG from the data by finding the t_{ff} from its assumed density. In light of this, considering Equations (11) and (3), the t_{ff} is calculated for the above-obtained masses. Now using Equation (4) as a fundamental, I calculated the efficiency as:

$$\epsilon_{\mathrm{ff}}(\mathrm{O\,II}) = \frac{\dot{M}(\mathrm{O\,II})t_{\mathrm{ff}}(\mathrm{O\,II})}{M_c(\mathrm{O\,II})}, \tag{12}$$

$$\epsilon_{\mathrm{ff}}(\mathrm{H}_\alpha) = \frac{\dot{M}(\mathrm{H}_\alpha)t_{\mathrm{ff}}(\mathrm{H}_\alpha)}{M_c(\mathrm{H}_\alpha)}, \tag{13}$$

$$\epsilon_{\mathrm{ff}}(\mathrm{IR}) = \frac{\dot{M}(\mathrm{IR})t_{\mathrm{ff}}(\mathrm{IR})}{M_c(\mathrm{IR})}, \tag{14}$$

$$\epsilon_{\mathrm{ff}}(1.4\ \mathrm{GHz}) = \frac{\dot{M}(1.4\ \mathrm{GHz})\,t_{\mathrm{ff}}(1.4\ \mathrm{GHz})}{M_c(1.4\ \mathrm{GHz})}, \tag{15}$$

where ϵ_{ff}(O II), $\epsilon_{\mathrm{ff}}(\mathrm{H}_\alpha)$, ϵ_{ff}(IR) and ϵ_{ff}(1.4 GHz) are SFEs from the respective MC mass, t_{ff} time and SFR.

The cloud mass derived from (O II) illustrates the ϵ_{ff} of BCGs, as shown in Figure 3. This figure indicates a peak efficiency of 0.425%. Variations in the ϵ_{ff} values can arise from differences in observational methods. Therefore, it is essential to conduct observations from various angles and across different spectra to obtain a more comprehensive understanding of efficiency. The ϵ_{ff} in BCGs, as represented by Figure 4, is measured in relation to cloud mass using H_α. The figure clearly indicates that the maximum ϵ_{ff} achieved is 0.675% in terms of cloud mass measured by H_α. The plot presented in Figure 5 illustrates the relationship between the ϵ_{ff} of BCGs and cloud mass as observed in the IR spectrum. It can be observed from Figure 5 that the highest efficiency recorded is 0.725% for the IR spectrum. Figure 6 depicts the correlation between the ϵ_{ff} of BCGs and cloud mass as determined by radio continuum measurements. The data indicate that the peak ϵ_{ff} reaches 0.825% at a frequency of 1.4 GHz. Additionally, Figure 7 confirms that the maximum ϵ_{ff} occurs at the 1.4 GHz radio continuum, also around 0.825%. Furthermore, Figure 8 reinforces this finding, showing that the highest ϵ_{ff} is similarly recorded at a 1.4 GHz radio continuum of approximately 0.825. The data presented in Figure 9 reinforce the observation that the maximum SFR is achieved at a frequency of 1.4 GHz in the radio continuum. Additionally, Figures 7–9 indicate that the highest values of ϵ_{ff} and SFR coincide with the 1.4 GHz radio continuum, highlighting the significance of monitoring star-forming regions across different wavelengths of the electromagnetic spectrum. Figure 10 illustrates that the relationship between the efficiencies of star formation across different spectra can be analyzed from an alternative viewpoint.

The data presented in the figures demonstrate that the SFE of a cloud within a BCG, when assessed through various methodologies, yields results that are relatively consistent with one another, despite minor discrepancies arising from the differences in observational techniques employed. Figure 11 indicates that the maximum depletion time occurs at [O II]3727, which has the potential to decrease the ϵ_{ff}. The data demonstrate that the ϵ_{ff} of galaxies vary depending on the spectral range utilized for analysis, with the computed efficiencies also changing based on the particular type of spectrum observed in these galaxies.

5. Conclusion

The study of SFE of BCGs in t_{ff} was carried out through an in-depth examination of observational data sourced from the catalog by Kong (2004), which included metrics on SFRs and depletion timescales. Utilizing this information, the remaining parameters, such as the mass of the cloud and the efficiencies of star formation, were subsequently computed. It is essential to note that the data set did not include any calculations or forecasts related to the ϵ_{ff} of MCs in these galaxies. As a result, my aim was to determine the SFE during the t_{ff} of the clouds by utilizing the spectrum through which the galaxy was observed. This involved calculating the t_{ff} and MCs masses, using the SFR and depletion time available in the data set. Ultimately, I applied the fundamental equation to assess the SFE in relation to t_{ff}. Through this approach, I managed to recognize the SFE in t_{ff} associated with the MC masses derived from various spectra, suggesting that the ϵ_{ff} of star formation varies depending on the particular spectrum employed for observation.

This paper utilized H_α, [O II]3727, IR, radio (1.4 GHz) luminosities, and neutral hydrogen (H I) gas masses to estimate the mass of the star-forming gas and to calculate the SFE of BCGs. Subsequently, it examined the variations in ϵ_{ff} derived from the aforementioned luminosities. The findings reveal that the ϵ_{ff} calculated from radio (1.4 GHz) luminosities tend to be somewhat higher than those derived from H_α, [O II]3727, and IR measurements. Therefore, it is advisable to investigate the SFE of these galaxies using a variety of spectral data. The calculation shows the peak value of ϵ_{ff} is attained for the cloud when observed at 1.4 GHz radio continuum spectrum which is indicated in Figure 6, i.e., $\epsilon_{\mathrm{ff}} \sim$ 0.825%.

These findings suggest that the efficiencies associated with star-forming clouds fluctuate across various wavelengths of the electromagnetic spectrum. Consequently, it is crucial to highlight the significance of employing multi-wavelength telescopes to observe a particular star-forming region, as this approach facilitates the acquisition of comprehensive data necessary for the precise interpretation of the SFR and SFE. The findings of this research reveal that the highest recorded value of $\epsilon_{\rm ff}$ was 0.825%, with an average value near 0.66%. These figures (Figures 3–11) align with the range of SFEs referenced by multiple authors in the introductory section. It is imperative to explore the factors that influence the variability of $\epsilon_{\rm ff}$ in a cloud when observed across different wave bands.

References

Bertram, E., Glover, S. C., Clark, P. C., Ragan, S. E., & Klessen, R. S. 2016, MNRAS, 455, 3763

Bolatto, A. D., Leroy, A. K., Rosolowsky, E., Walter, F., & Blitz, L. 2008, ApJ, 686, 948

Evans, N. J., II, Dunham, M. M., Jørgensen, J. K., et al. 2009, ApJS, 181, 321

Fujii, M. S., & Zwart, S. P. 2016, ApJ, 817, 4

Gallego, J., Zamorano, J., Aragon-Salamanca, A., et al. 1995, ApJL, 455, L1

García-Burillo, S., Usero, A., Alonso-Herrero, A., et al. 2012, A&A, 539, A8

Heiderman, A., Evans, N. J., II, Allen, L. E., Huard, T., & Heyer, M. 2010, ApJ, 723, 1019

Izotov, Y. I., Lipovetskii, V. A., Guseva, N. G., Kniazev, A. Y., & Stepanian, J. A. 1990, Natur, 343, 238

Kong, X. 2004, A&A, 425, 417

Kennicutt, R. C. 1998, ARA&A, 36, 189

Kumssa, G. M., & Tessema, S. B. 2021, in IAU Symp. 356, Nuclear Activity in Galaxies Across Cosmic Time, ed. M. Pović et al. (Cambridge: Cambridge Univ. Press), 388

Kumssa, G. M., & Tessema, S. B. 2022, NewA, 96, 101854

Krumholz, M. R., Dekel, A., & McKee, C. F. 2011, ApJ, 745, 69

Krumholz, M. R., & McKee, C. F. 2005, ApJ, 630, 250

Krumholz, M. R., & Tan, J. C. 2007, ApJ, 654, 304

Krumholz, M. R., & Thompson, T. A. 2013, MNRAS, 434, 2329

Kunth, D., & Östlin, G. 2000, A&ARv, 10, 1

Madau, P., Ferguson, H. C., Dickinson, M. E., et al. 1996, MNRAS, 283, 1388

Mo, H., Van den Bosch, F., & White, S. D. M. 2010, Galaxy Formation and Evolution (Cambridge: Cambridge Univ. Press)

Mac Low, M. M. 2016, in IAU Symp. 315, From Interstellar Clouds to Star-Forming Galaxies: Universal Processes?, ed. F. Van der Tak, P. Jablonka, & P. Andre (Cambridge: Cambridge Univ. Press), 1

Murray, N. 2011, ApJ, 729, 133

Myers, P. C., Dame, T. M., Thaddeus, P., et al. 1986, ApJ, 301, 398

Pettini, M., Kellogg, M., Steidel, C. C., et al. 1998, ApJ, 508, 539

Robitaille, T. P., & Whitney, B. A. 2010, ApJL, 710, L11

Solomon, P. M., Rivolo, A. R., Barrett, J., Yahil, A, et al. 1987, ApJ, 319, 730

Steidel, C. C., Adelberger, K. L., Giavalisco, M., et al. 1999, ApJ, 519, 1

Thuan, T. X., Izotov, Y. I., & Lipovetsky, V. A. 1996, ApJ, 463, 120